Desalination and Water Treatment
www.deswater.com

doi: 10.5004/dwt.2017.20602

74 (2017) 346–353
May

Photocatalytic degradation of methylene blue dye by F-doped Co_3O_4 nanowires

Tariq R. Sobahi[a,*], M.S. Amin[b,c], Reda M. Mohamed[a,d]

[a]*Department of Chemistry, Faculty of Science, King Abdulaziz University, PO Box 80203, 21589 Jeddah, Saudi Arabia, emails: tsohabi@gmail.com (T.R. Sobahi), redama123@yahoo.com (R.M. Mohamed)*
[b]*Department of Basic Sciences and Technology, Community College, Taibah University, Saudi Arabia, email: mohamedsamin@hotmail.com*
[c]*Chemistry Department, Faculty of Science, Ain Shams University, Cairo, Egypt*
[d]*Advanced Materials Department, Central Metallurgical R&D Institute, CMRDI, PO Box 87, Helwan, Cairo, Egypt*

Received 30 October 2016; Accepted 16 February 2017

ABSTRACT

The hydrothermal method was used to prepare Co_3O_4 with different shapes by varying concentration of NaOH from 3 to 12 M. Shape of Co_3O_4 was found to be nanowire by using 9 M NaOH. Fluorine was doped into the surface of Co_3O_4 nanowire by impregnation method. Doping of fluorine into the surface of Co_3O_4 nanowire decreases bandgap of Co_3O_4 nanowire from 2.49 to 2.32 eV as a result of the blocking of some pores of Co_3O_4 nanowire. The surface area of undoped Co_3O_4 nanowire is higher than that of doped Co_3O_4 nanowire. Doping of fluorine into surface of Co_3O_4 nanowire enhances the photocatalytic performance of Co_3O_4 nanowire toward degradation of methylene blue dye under visible light.

Keywords: Co_3O_4; Hydrothermal; Fluorine; Methylene blue dye

1. Introduction

One of the biggest issues, which is encountered in most countries of the world nowadays that are facing severe water shortage problem, is water purification. It is estimated that more than one billion people suffer from lack of safe drinking water [1].

Textile manufacture is considered one of the major origins of environmental contamination; attention has been paid to remove dyestuffs from wastewater in the past decades [2]. Therefore, removal of colored wastewater is a crucial issue in the recent years. The traditional techniques involved in color removal are filtration, chemical precipitation and adsorption on organic or inorganic matrices.

Various investigations have been studied for methylene blue (MB) dye removal from the aqueous solution, such as adsorption of MB onto clay [3], using the waste of Abu-Tartour phosphate to adsorb MB [4], adsorption study of MB on black cherries after its chemical activation [5], applying Jordanian diatomite to remove MB dye [6], employing hazelnut shell for MB adsorption [7], flamboyant pods [8], various fruit peels [9], removal of MB dye via its adsorption on coir pith carbon [10], MB dye sorption using Egyptian rice hull [11], using vetiver roots activated carbon to adsorb MB dye [12], garlic peel [13], citrus fruit peel [14], banana leaves [15] and removal of MB from effluent using montmorillonite clay [16]. Each method exhibits several advantages and disadvantages that limit its application in industrial fields. Processes like coagulation and adsorption are low-cost processes but they have a disadvantage of transferring the primary pollutants into secondary ones, which need further treatment, and in some cases, the by-products may be more toxic and more hazardous than the dye itself [17].

Recently, the concentration on heterogeneous photocatalysis using semiconductors to remove organic contaminants from the wastewater has been grown up. The main advantage of photocatalysis is that it provides a more environmentally sustainable solution such that the pollutants are destroyed without a need for subsequent disposal of the wastes.

* Corresponding author.

Various types of semiconductors were involved in photocatalytic degradation of several hazardous organic pollutants [18,19]. Among these semiconductors, TiO_2 has been successfully used as photocatalyst as a result of its higher activity, non-toxicity, thermal and chemical stability, commercial availability and low costs. On the other hand, TiO_2 is active only under ultraviolet (UV) light, which is considered a primary disadvantage that limits its industrial applications. Moreover, the high rate of recombination of photogenerated electron–hole pairs that resulting in low photo quantum efficiency had been considered as the second disadvantage of using TiO_2 as photocatalyst [20].

The optical features of titania were improved by doping it with transition metal elements to increase the absorption range of the catalyst to visible region. However, pure, doped and mixed titanium oxide prepared in micro-scale suffer from low surface area and irregular particle and pore structure that hamper its applications in various industrial processes. The recent trends aimed to focus on the development of new materials at the atomic or molecular scale to achieve a high degree of photocatalytic reactivity.

Recently, metal oxides [21], sulfides [22,23], $BiVO_4$ or g-C_3N_4/$BiVO_4$ nanocomposites [24–26], Bi_2WO_6 or C_3N_4/Bi_2WO_6 composites [27,28], g-C_3N_4 or g-C_3N_4 hybrid nanocomposites [29–32], WO_3 or WO_3/g-C_3N_4 nanocomposites [33–35], $SrTiO_3$ [36,37], etc. have been used for degradation of organic pollutants.

Co_3O_4 has attracted much attention as a p-type semiconductor having interesting electromagnetic properties [38–40], its catalytic ability for oxidation of CO [41], dibromomethane [42] and oxidation of 1,2-dichloroethane [43]. In some studies Co_3O_4 has also been reported to be very active for degradation of hazardous gases like NO_x [44], catalytic ozonation for benzophenone-3 [45] and efficient photoelectrochemical water splitting [46] as well its use for catalytic oxidation of formaldehyde [47] and visible light degradation of organic pollutants [48–52].

Numerous methods have been adopted to prepare these nanomaterials as microwave irradiation, sol–gel process, solution combustion, solvothermal method, etc. [53,54]. These preparation methods require complicated equipment and severe reaction environment. The process simplicity of hydrothermal preparation method makes it widely applicable compared with other convenient chemical synthesis methods for nanoscale materials [55–57]. The advantages offered by this technique include simple preparation, comparatively low process temperatures, shorter reaction times and nanomaterial products with uniform particle size range. In this project, Co_3O_4 nanowire was prepared by a hydrothermal method using 12 M NaOH for first time, and fluorine was doped into surface of Co_3O_4 nanowire by impregnation method to decrease e–h recombination rate and shift absorption edge of Co_3O_4 to high value of wavelength. The photocatalytic performance of F/Co_3O_4 nanowire was studied by degradation of MB dye under visible light.

2. Experimental setup

2.1. Preparation of photocatalysts

All chemicals were handled without any clarification. Cobalt(II) acetate tetrahydrate, sodium hydroxide pellets and NH_4F were obtained from Aldrich, USA. For comparison, P_{25} was purchased from Degussa, Germany. Co_3O_4 with different shapes was prepared via the hydrothermal method by varying sodium hydroxide concentration from 3 to 12 M. This method can be described as follows: 5 g of cobalt(II) acetate tetrahydrate was dissolved in 10 mL of sodium hydroxide solution, and concentration of sodium hydroxide was varied from 3 to 12 M. The resultant mixture was hydrothermally treated in an autoclave at 200°C overnight. The temperature of the autoclave was decreased gradually; the obtained materials were dried and cleaned up in many intervals with deionized water and finally were left to dry at 100°C for 24 h. Fluorine was doped on surface of Co_3O_4 nanowires by impregnation method as in the following steps: 2 g of Co_3O_4 nanowire was impregnated in an aqueous solution containing 0.08 g of NH_4F, and the resultant mixture was stirred for 24 h at room temperature. The obtained materials were dried and washed several times with deionized water and finally were dried at 50°C for 24 h.

2.2. Characterization techniques

A Bruker axis D8 with Cu Kα radiation (λ = 1.540 Å) was applied to determine thin film phase and its crystallite size. A Nova 2000 series Chromatech apparatus was employed to determine thin film specific surface area; the samples were treated for 2 h under vacuum at 100°C before taking the measurements. UV–visible (UV–Vis) diffuse reflectance spectroscopy was used to display the performance of the bandgap of the samples. The spectroscopy was performed in air at room temperature using a UV/Vis/NIR spectrophotometer (V-570, JASCO, Japan) in the wavelength range of 200–800 nm. A JEOL-JEM-1230 microscope was used for the transmission electron microscopy (TEM) analysis. The samples were set up in a suspension of ethanol and subjected to half an hour of ultrasonication. A small amount of solution was placed on a copper grid coated with carbon and left to dry. Once the solution was dried, the sample was loaded into the TEM. A Thermo Scientific K-ALPHA XPS was used to perform the X-ray photoelectron spectroscopy (XPS). A Shimadzu RF-5301 fluorescence spectrophotometer was used for recording the photoluminescence (Pl) emission spectra.

2.3. Photocatalysis experiment

A Xenon lamp with a power of 300 W, an intensity of 0.96 W/cm^2 and a cut-off filter of 420 nm was used to study the photocatalytic degradation of MB dye. Prior to the photocatalytic test, the photocatalyst was suspended in an aqueous solution of MB dye in a 500-mL reactor. Then, the obtained mixture was stirred for 30 min in the dark to establish the adsorption–desorption equilibrium. At different time intervals, a sample from the mixture was taken and filtrated for analysis. The removed sample was then analyzed by determining its absorbance at 664 nm using a spectrophotometer.

3. Results and discussion

3.1. Characterization of Co_3O_4

3.1.1. TEM examination

Figs. 1(A)–(D) show TEM images of Co_3O_4 samples, prepared using (3, 6, 9 and 12 M, respectively) of NaOH solution.

The results reveal that the shape of Co_3O_4 is nanospherical when concentration of sodium hydroxide is 3 M as shown in Fig. 1, and the shape of Co_3O_4 is irregular nanospherical when concentration of sodium hydroxide is 6 M as shown in Fig. 1(B). Moreover, the Co_3O_4 nanoparticles have nanowire shape when concentration of sodium hydroxide is 9 M as shown in Fig. 1(C), while when concentration of sodium hydroxide is 12 M, the Co_3O_4 nanoparticles have a mixture of nanowire and nanosphere shapes as shown in Fig. 1(D).

3.1.2. XRD examination

Figs. 2(A)–(D) show X-ray diffraction (XRD) peaks of Co_3O_4 samples, prepared using (3, 6, 9 and 12 M, respectively) of NaOH solution. The results reveal that all samples are composed of Co_3O_4 (Joint Committee on Powder Diffraction Standards card no. 78-1970), and sodium hydroxide concentration has no significant effect on the structure of Co_3O_4.

3.1.3. UV–Vis spectra examination

Figs. 3(A)–(D) show UV–Vis spectra for Co_3O_4 samples, prepared using (3, 6, 12 and 9 M, respectively) of NaOH solution. The results indicate that all Co_3O_4 samples absorb in the visible region. Also, we notice that the absorption edge of Co_3O_4 is affected by sodium hydroxide concentration. It is clear that increasing sodium hydroxide concentration from 3 to 9 M increases the absorption edge of Co_3O_4 from 420 to 497 nm, respectively, as shown in Figs. 3(A) and (D). However, increasing sodium hydroxide concentration from 9 to 12 M decreases the absorption edge of Co_3O_4 from 497 to 466 nm, respectively, as shown in Figs. 3(D) and (C). These findings may be attributed to the change of the Co_3O_4 shape from nanowire to a mixture of nanowire and nanosphere as a result of increasing sodium hydroxide concentration from 9 to 12 M. The values of bandgap energy of Co_3O_4 prepared at 3, 6, 9 and 12 M of NaOH solution are 2.95, 2.86, 2.49 and 2.66 eV, respectively.

3.1.4. Pl spectra examination

Figs. 4(A)–(D) show Pl spectra for Co_3O_4 samples, prepared using (3, 6, 12 and 9 M, respectively) of NaOH solution. The results reflect that Pl peak intensity of Co_3O_4 is affected by sodium hydroxide concentration. In fact, increasing sodium hydroxide concentration from 3 to 9 M leads to a decrease in the Pl peak intensity as shown in Figs. 3(A) and (D). On contrary, when sodium hydroxide concentration increases from 9 to 12 M, the Pl peak intensity increases as shown in Figs. 3(D) and (C). This increase may be attributed to the change of Co_3O_4 shape from nanowire to a mixture of nanowire and nanosphere upon increasing sodium hydroxide concentration from 9 to 12 M.

3.1.5. Specific surface area analysis

Brunauer–Emmett–Teller (BET) specific surface areas of Co_3O_4 samples prepared using different sodium hydroxide concentrations are given in Table 1. The results reveal that concentration of sodium hydroxide is a dominant factor in determining shape, bandgap and the BET surface area of the prepared Co_3O_4 samples. It can be seen that the values of BET

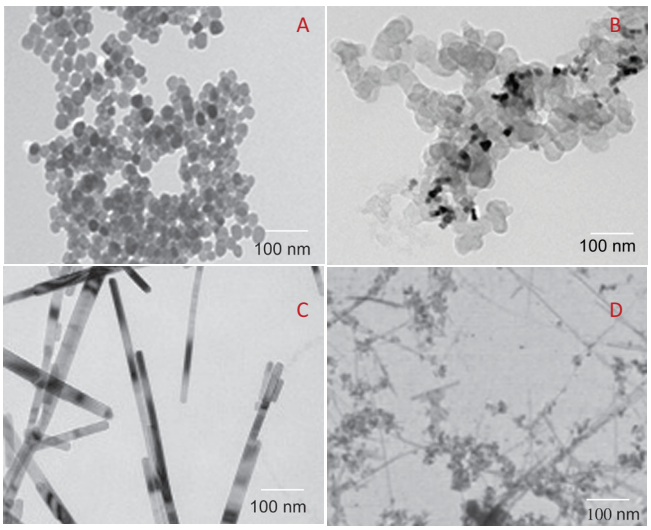

Fig. 1. (A)–(D) TEM images of Co_3O_4 samples, prepared using (3, 6, 9 and 12 M, respectively) of NaOH solution.

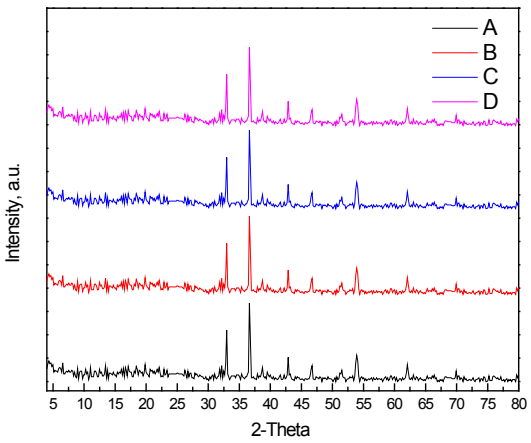

Fig. 2. (A)–(D) XRD patterns of Co_3O_4 samples, prepared using (3, 6, 9 and 12 M, respectively) of NaOH solution.

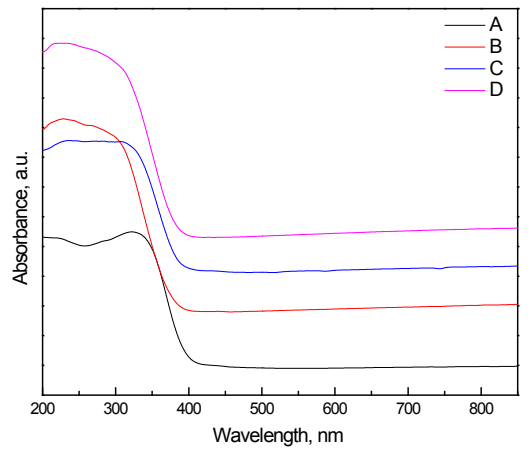

Fig. 3. (A)–(D) UV–Vis spectra for Co_3O_4 samples, prepared using (3, 6, 12 and 9 M, respectively) of NaOH solution.

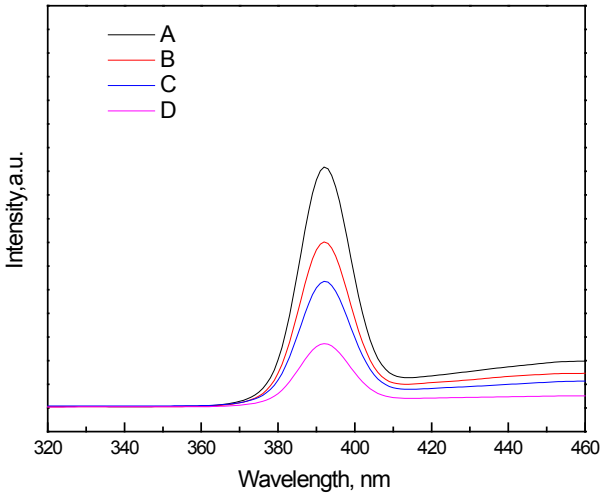

Fig. 4. (A)–(D) Pl spectra for Co_3O_4 samples, prepared using (3, 6, 12 and 9 M, respectively) of NaOH solution.

Table 1
BET surface area of Co_3O_4 samples prepared at different sodium hydroxide concentrations

Concentration of sodium hydroxide, M	SBET (m^2/g)
3	30
6	25
9	60
12	45

specific surface area of Co_3O_4 prepared at 3, 6, 9 and 12 M of NaOH solution are 30, 25, 60 and 45 m^2/g, respectively.

3.2. Characterization of the F/Co_3O_4 nanocomposite

3.2.1. TEM examination

Figs. 5(A) and (B) show TEM images of the prepared Co_3O_4 and F/Co_3O_4, respectively. The results reveal that doping of fluorine has no significant effect on the shape of Co_3O_4, i.e., shapes of Co_3O_4 and F/Co_3O_4 are nanowire. Also, we notice that F was dispersed on the surface of Co_3O_4 nanowire.

3.2.2. XRD examination

Figs. 6(A) and (B) show XRD patterns of the prepared Co_3O_4 and F/Co_3O_4, respectively. The results reveal that doping of fluorine has no significant effect on the XRD pattern of Co_3O_4, which means that the weight percentage of fluorine is low to some extent to be detected by XRD and/or F is well dispersed on surface of Co_3O_4 nanowire; this result agrees with the results obtained from TEM analysis.

3.2.3. UV–Vis spectra examination

Figs. 7(A) and (B) show the UV–Vis spectra of the prepared Co_3O_4 and F/Co_3O_4, respectively. The results reveal that

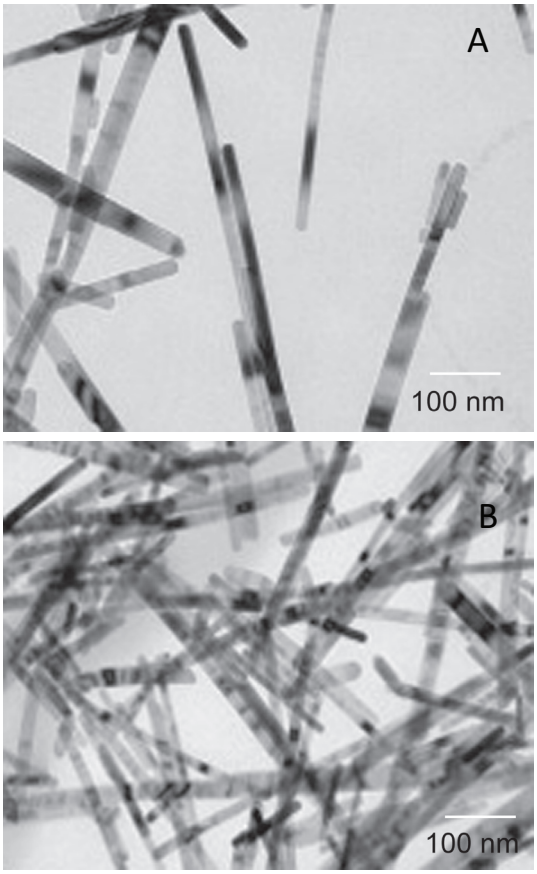

Fig. 5. (A) and (B) TEM images of Co_3O_4 and F/Co_3O_4, respectively.

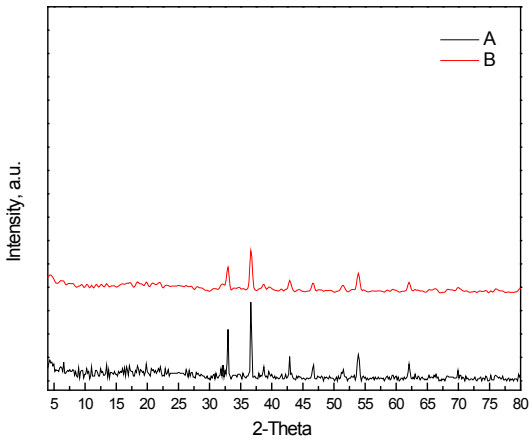

Fig. 6. (A) and (B) XRD patterns of Co_3O_4 and F/Co_3O_4, respectively.

both Co_3O_4 nanowire and F/Co_3O_4 nanocomposite samples absorb in the visible region. Also, we notice that the absorption edge of Co_3O_4 is affected by fluorine doping. It could be concluded that doping of fluorine increases absorption edge of Co_3O_4 from 497 to 535 nm as shown in Figs. 7(A) and (B). The values of bandgap energy of Co_3O_4 nanowire and F/Co_3O_4 nanocomposite are 2.49 and 2.32 eV, respectively.

3.2.4. Pl spectra examination

Fig. 8 shows the Pl spectra of Co_3O_4 (A) and F/Co_3O_4 (B). The results reveal that Pl peak intensity Co_3O_4 is affected by doping of fluorine. Doping of fluorine decreases the peak intensity Co_3O_4 as shown in Figs. 8(A) and (B).

3.2.5. XPS examination

Fig. 9 shows XPS spectra of F1s for F/Co_3O_4 nanocomposite. The results reveal that fluorine is present as fluoride ion due to presence of peak of F1s at 684.4 eV. Therefore, fluorine is well dispersed into the surface of Co_3O_4 nanowire.

3.2.6. Specific surface area analysis

The values of BET specific surface area of Co_3O_4 nanowire and F/Co_3O_4 nanocomposite were found to be 60 and 50 m^2/g, respectively. The decrease in surface area of Co_3O_4 nanowire by fluorine doping could be explained as a result of blocking of some pores of Co_3O_4.

3.3. Photocatalytic performance for the degradation of MB dye

3.3.1. Effect of the photocatalyst type

Fig. 10 shows the effect of the photocatalyst type on the photocatalytic degradation of MB dye, where the photocatalyst is (A) P_{25} Degussa; (B) Co_3O_4 using 3 M NaOH; (C) Co_3O_4 using 6 M NaOH; (D) Co_3O_4 using 12 NaOH; (E) Co_3O_4 using 9 M NaOH and (F) F/Co_3O_4 nanocomposite. The photocatalytic reaction was carried out under the following conditions: 1,000 mL volume of MB dye; 100 ppm concentration of MB dye; irradiation using visible light origin; 1.0 g photocatalyst dose and 60 min photocatalytic reaction time. The results reveal that NaOH concentration plays an important role in determining properties of the prepared Co_3O_4 (shape, surface area and bandgap). Therefore, sodium hydroxide concentration plays an important role on the photocatalytic activity of Co_3O_4 for degradation of MB dye. In fact, increasing sodium hydroxide concentration from 3 to 9 M leads to an increase in the photocatalytic activity from 9% to 55%, respectively. Whereas, increasing sodium hydroxide concentration from 9 to 12 M leads to a decrease in the photocatalytic activity from 55% to 45%, respectively, due to the shape change of Co_3O_4 from nanowire, which has high surface area and low value of bandgap, to a mixture of nanowire and nanosphere, which has low surface area and high value of bandgap. Also, we notice that doping of fluorine on the surface of Co_3O_4 nanowire increases photocatalytic activity from 55% to 86%, respectively. And so, F/Co_3O_4 nanocomposite has the highest photocatalytic activity and the smallest bandgap. Table 2 summarizes the rate constant of reaction kinetics for each sample type.

3.3.2. Effect of the photocatalyst dose

The effect of F/Co_3O_4 amount on the photocatalytic destruction of MB dye is illustrated in Fig. 11. The photocatalytic reaction was carried out under the following conditions: 1,000 mL volume of MB dye; 100 ppm concentration of MB dye; F/Co_3O_4 photocatalyst; visible light source of irradiation; 0.5–2.5 g photocatalyst dose and 60 min photocatalytic

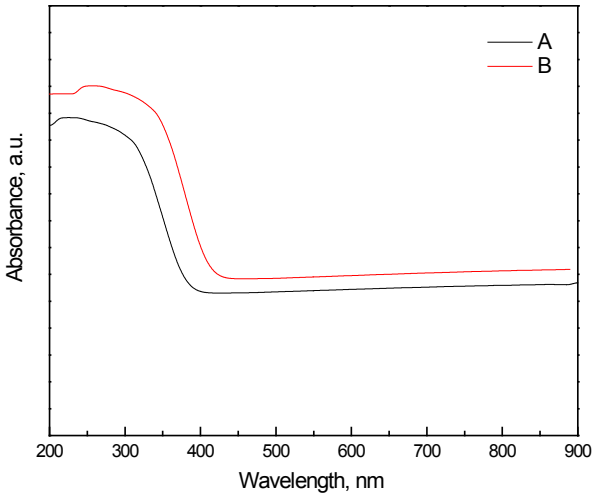

Fig. 7. (A) and (B) UV–Vis spectra of Co_3O_4 and F/Co_3O_4, respectively.

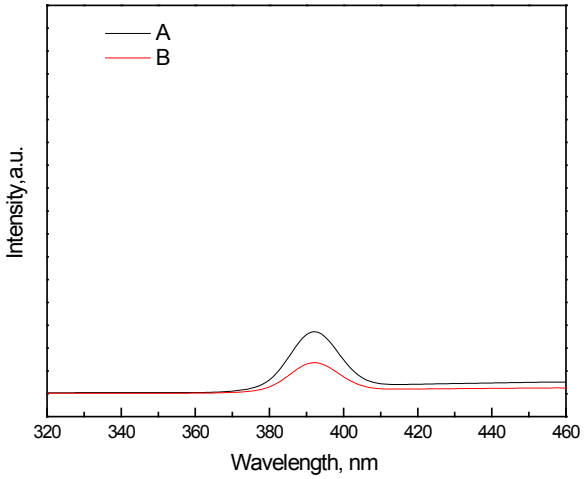

Fig. 8. (A) and (B) Pl spectra of Co_3O_4 and F/Co_3O_4, respectively.

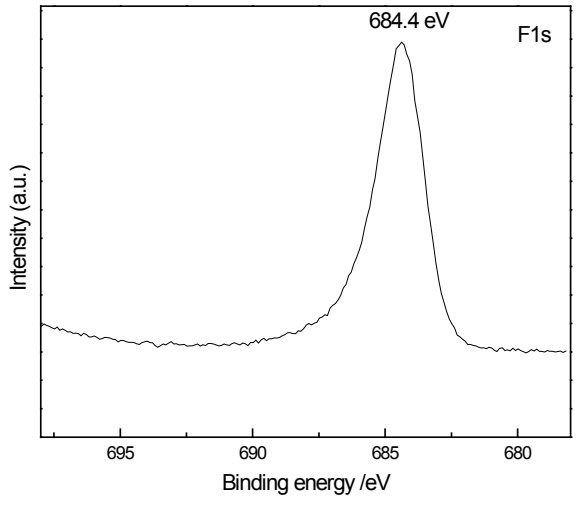

Fig. 9. XPS spectra of F1s for F/Co_3O_4 nanocomposite.

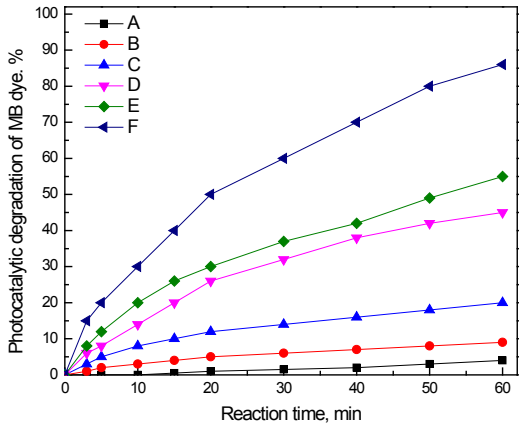

Fig. 10. Photocatalyst type and its effect on the photocatalytic destruction of MB dye, where the photocatalyst is (A) P_{25} Degussa; (B) Co_3O_4 using 3 M NaOH; (C) Co_3O_4 using 6 M NaOH; (D) Co_3O_4 using 12 M NaOH; (E) Co_3O_4 using 9 M NaOH and (F) F/ Co_3O_4 nanocomposite.

Table 2
Rate constants of reaction kinetics for photocatalyst type and its effect on the photocatalytic destruction of MB dye, where the photocatalyst is P_{25} Degussa; Co_3O_4 using 3 M NaOH; Co_3O_4 using 6 M NaOH; Co_3O_4 using 12 M NaOH; Co_3O_4 using 9 M NaOH and F/Co_3O_4 nanocomposite

Sample	$k \times 10^{-5}$, min^{-1}
P_{25} Degussa	40
Co_3O_4 using 3 M NaOH	50
Co_3O_4 using 6 M NaOH	80
Co_3O_4 using 9 M NaOH	120
Co_3O_4 using 12 M NaOH	110
F/Co_3O_4 nanocomposite	2,000

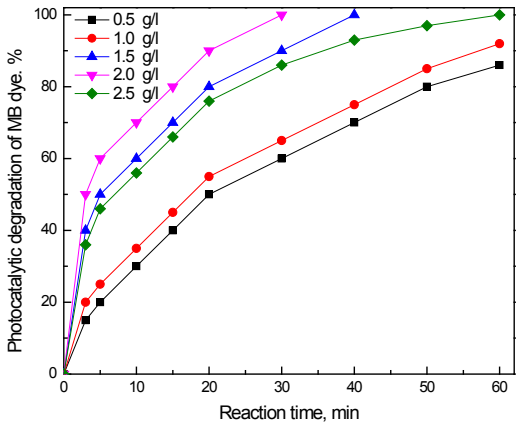

Fig. 11. Effect of F/Co_3O_4 dose on the photocatalytic degradation of MB dye.

reaction time. The results reveal that increasing photocatalyst dose from 0.5 to 1.0 g leads to an increase in the photocatalytic activity from 86% to 92% after 60 min. In addition, increasing photocatalyst dose from 1.0 to 1.5 g leads to an increase in the photocatalytic activity from 92% to 100% and a decrease in the photocatalytic reaction time from 60 to 40 min. On the other hand, increasing photocatalyst dose from 1.5 to 2.0 g leads to a decrease in the photocatalytic reaction time from 40 to 30 min. On contradiction, increasing photocatalyst dose from 2.0 to 2.5 g leads to an increase in the photocatalytic reaction time from 30 to 60 min. These findings may be attributed to the hindering of the light penetration during photocatalysis and decreasing the available active sites for the photocatalytic reaction as a result of the large weight of the photocatalyst, which, by its role, leads to a decreased overall photocatalytic activity. Table 3 summarizes the rate constant of reaction kinetics for each sample type.

Table 3
Rate constants of reaction kinetics for effect of catalyst amount on degradation of MB dye

Sample, g/L	$k \times 10^{-5}$, min^{-1}
0.5	2,000
1.0	4,500
1.5	6,020
2.0	6,300
2.5	4,000

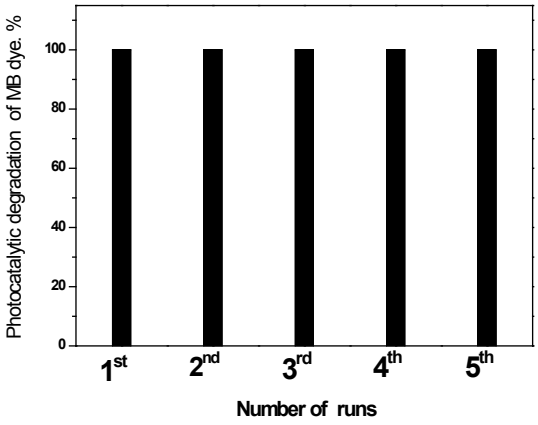

Fig. 12. Recycle of the F/Co_3O_4 nanocomposite for the photocatalytic degradation of MB dye.

3.3.3. Recycling of the photocatalyst

Fig. 12 illustrates recycling and reusing of the F/Co_3O_4 nanocomposite for the photocatalytic degradation of MB dye. The results reveal that photocatalytic activity of F/Co_3O_4 nanocomposite is almost unchanged after being reused five times.

4. Conclusions

The main conclusions derived from this study are:

- Sodium hydroxide concentration plays an important role on controlling the shape, bandgap and BET surface area of the Co_3O_4 photocatalyst.
- All Co_3O_4 and F/Co_3O_4 samples absorb in the visible region, whereas their absorption edges are different.

- Doping of fluorine has no significant effect on either the shape or XRD pattern of Co_3O_4 photocatalyst, whereas it affects its bandgap, surface area and Pl peak intensity.
- Sodium hydroxide concentration plays an important role on the photocatalytic activity of Co_3O_4 for degradation of MB dye.
- Increasing F/Co_3O_4 dose from 0.5 to 2 g increases its photocatalytic activity of the photocatalyst for degradation of MB dye, whereas further increase in the photocatalyst dose decreases its photocatalytic activity.

Acknowledgment

This project was funded by Saudi Basic Industries Corporation (SABIC) and the Deanship of Scientific Research (DSR) at King Abdulaziz University, Jeddah, under grant no. S-77-130-37. The authors, therefore, acknowledge with thanks SABIC and DSR for technical and financial support.

References

[1] S. Malato, P. Fernandez-Ibañez, M.I. Maldonado, J. Blanco, W. Gernjak, Decontamination and disinfection of water by solar photocatalysis: recent overview and trends, Catal. Today, 147 (2009) 1–59.
[2] C.-H. Weng, Y.-F. Pan, Adsorption of a cationic dye (methylene blue onto spent activated clay, J. Hazard. Mater., 144 (2007) 355–362.
[3] A. Gürses, Ç. Doğar, M. Yalçın, M. Açıkyıldız, R. Bayrak, S. Karaca, The adsorption kinetics of the cationic dye, methylene blue, onto clay, J. Hazard. Mater., 131 (2006) 217–228.
[4] G.F. Malash, M.I. El-Khaiary, Methylene blue adsorption by the waste of Abu-Tartour phosphate rock, J. Colloid Interface Sci., 348 (2010) 537–545.
[5] J.M.R.R. Arana, R.R. Mazzoco, Adsorption studies of methylene blue and phenol onto black stone cherries prepared by chemical activation, J. Hazard. Mater., 180 (2010) 656–661.
[6] M.A. Al-Ghouti, M.A.M. Khraisheh, M.N.M.Ahmad, S. Allen, Adsorption behavior of methylene blue onto Jordanian diatomite: a kinetic study, J. Hazard. Mater., 165 (2009) 589–598.
[7] M. Doğan, H. Abak, M. Alkan, Adsorption of methylene blue onto hazelnut shell: kinetics, mechanism and activation parameters, J. Hazard. Mater., 164 (2009) 172–181.
[8] A.M.M. Vargas, A.L. Cazetta, M.H. Kunita, T.L. Silva, V.C. Almeida, Adsorption of methylene blue on activated carbon produced from flamboyant pods (*Delonix regia*): study of adsorption isotherms and kinetic models, Chem. Eng. J., 168 (2011) 722–730.
[9] F.S. Hashem, M.S. Amin, Adsorption of methylene blue by activated carbon derived from various fruit peels, Desal. Wat. Treat., 57 (2016) 22573–22584.
[10] D. Kavitha, C. Namasivayam, Experimental and kinetic studies on methylene blue adsorption by coir pith carbon, Bioresour. Technol., 98 (2007) 14–21.
[11] M.M. El-Halwany, Study of adsorption isotherms and kinetic models for methylene blue adsorption on activated carbon developed from Egyptian rice hull (Part II), Desalination, 250 (2010) 208–213.
[12] S. Altenor, B. Carene, E. Emmanuel, J. Lambert, J.-J. Ehrhardt, S. Gaspard, Adsorption studies of methylene blue and phenol onto vetiver roots activated carbon prepared by chemical activation, J. Hazard. Mater., 165 (2009) 1029–1039.
[13] B.H. Hameed, A.L. Ahmad, Batch adsorption of methylene blue from aqueous solution by garlic peel, an agricultural waste biomass, J. Hazard. Mater., 164 (2009) 870–875.
[14] S. Dutta, A. Bhattacharyya, A. Ganguly, S. Gupta, S. Basu, Application of response surface methodology for preparation of low-cost adsorbent from citrus fruit peel and for removal of Methylene Blue, Desalination, 275 (2011) 26–36.
[15] R.R. Krishni, K.Y. Foo, B.H. Hameed, Adsorptive removal of methylene blue using the natural adsorbent- banana leaves, Desal. Wat. Treat., 52 (2014) 6104–6112.
[16] C.A.P. Almeida, N.A. Debacher, A.J. Downs, L. Cottet, C.A.D. Mello, Removal of methylene blue from colored effluents by adsorption on montmorillonite clay, J. Colloid Interface Sci., 332 (2009) 46–53.
[17] J.W. Lee, H.J. Chun, D.H. Jung, T. Kwak, W.G. Ramesh, H. Shim, Comparative studies on coagulation and adsorption as a pretreatment method for the performance improvement of submerged MF membrane for secondary domestic wastewater treatment, Sep. Sci. Technol., 40 (2005) 2613–2632.
[18] O. Carp, C.L. Huisman, A. Reller, Photoinduced reactivity of titanium dioxide, Prog. Solid State Chem., 32 (2004) 33–177.
[19] Z. Yanqing, S. Erwel, C. Zhinzhan, L. Wenjun, H. Xingfang, Influence of solution concentration on the hydrothermal preparation of titania crystallites, J. Mater. Chem., 11 (2001) 1547–1551.
[20] K. Hashimoto, H. Irie, A. Fujishima, TiO_2 photocatalysis: a historical overview and future prospects, Jpn. J. Appl. Phys., 44 (2005) 8269–8285.
[21] J. Das, D. Khushalani, Nonhydrolytic route for synthesis of ZnO and its use as a recyclable photocatalyst, J. Phys. Chem. C, 114 (2010) 8114–8114.
[22] A. Kudo, Development of photocatalyst materials for water splitting, Int. J. Hydrogen Energy, 31 (2006) 197–202.
[23] J.Z. Yang, J.W. Yu, J. Fan, D.P. Sun, W.H. Tang, X.J. Yang, Biotemplated preparation of CdS nanoparticles/bacterial cellulose hybrid nanofibers for photocatalysis application, J. Hazard. Mater., 189 (2011) 377–383.
[24] F.F. Abdi, R.V.D. Krol, Nature and light dependence of bulk recombination in Co-Pi-catalyzed $BiVO_4$ photoanodes, J. Phys. Chem. C, 116 (2012) 9398–9404.
[25] Y.X. Ji, J.F. Cao, L.Q. Jiang, Y.H. Zhang, Z.G. Yi, G–C_3N_4/$BiVO_4$ composites with enhanced and stable visible light photocatalytic activity, J. Alloys Compd., 590 (2014) 9–14.
[26] F. Guo, W.L. Shi, X. Lin, G.B. Che, Hydrothermal synthesis of graphitic carbon nitride–$BiVO_4$ composites with enhanced visible light photocatalytic activities and the mechanism study, J. Phys. Chem. Solids, 75 (2014) 1217–1222.
[27] Y.L. Tian, B.B. Chang, J.L. Lu, J. Fu, F.N. Xi, X.P. Dong, Hydrothermal synthesis of graphitic carbonnitride–Bi_2WO_6 hetero junctions with enhanced visible light photocatalytic activities, ACS Appl. Mater. Interfaces, 5 (2013) 7079–7085.
[28] H. Wang, J. Lu, F. Wang, W. Wei, Y. Chang, S. Dong, Preparation, characterization and photocatalytic performance of g-C_3N_4/Bi_2WO_6 composites for methyl orange degradation, Ceram. Int., 40 (2014) 9077–9086.
[29] X. Zhou, S.Y. Yao, Y.M. Long, Z.S. Wang, W.F. Li, Microwave-assisted synthesis and enhanced visible-light-driven photocatalytic property of g-C_3N_4/Bi_2S_3 nano composite, Mater. Lett., 145 (2015) 23–26.
[30] X.F. Wang, W.W. Mao, J. Zhang, Y.M. Han, C.Y. Quan, Q.X. Zhang, T. Yang, J.P. Yang, X.A. Li, W. Huang, Facile fabrication of highly efficient g-C_3N_4/$BiFeO_3$ nano composites with enhanced visible light photocatalytic activities, J. Colloid Interface Sci., 448 (2015) 17–23.
[31] F. Chen, Y.F. Hu, X.L. Jiang, S.G. Meng, X.L. Fu, Fabrication and characterization of novel Z-scheme photocatalyst WO_3/g-C_3N_4 with high efficient visible light photocatalytic activity, Mater. Chem. Phys., 149–150 (2015) 512–521.
[32] R.C. Pawar, V. Khare, C.S.Y. Lee, Hybrid photocatalysts using graphitic carbon nitride/cadmium sulfide/reduced grapheme oxide (g-C_3N_4/CdS/RGO) for superior photodegradation of organic pollutants under UV and visible light, Dalton Trans., 43 (2014) 12514–12527.
[33] S.F. Chen, Y.F. Hu, S.G. Meng, X.L. Fu, Study on the separation mechanisms of photogenerated electrons and holes for composite photocatalysts g-C_3N_4–WO_3, Appl. Catal., B, 150–151 (2014) 564–573.
[34] S.F. Chen, Y.F. Hu, X.L. Jiang, S.G. Meng, X.L. Fu, Fabrication and characterization of novel Z-scheme photocatalyst WO_3/g-C_3N_4 with high efficient visible light photocatalytic activity, Mater. Chem. Phys., 149–150 (2015) 512–521.

[35] J.L. Zhao, Z.Y. Ji, X.P. Shen, H. Zhou, L.B. Ma, Facile synthesis of WO_3 nanorods/g-C_3N_4 composites with enhanced photocatalytic activity, Ceram. Int., 41 (2015) 5600–5606.
[36] S. Kumar, S. Tonda, A. Baruah, B. Kumar, V. Shanker, Synthesis of novel and stable g-C_3N_4/N-doped $SrTiO_3$ hybrid nano composites with improved photo current and photocatalytic activity under visible light irradiation, Dalton Trans., 43 (2014) 16105–16114.
[37] X. Chen, P.F. Tan, B.H. Zhou, H.G. Dong, J. Pan, X. Xiong, A green and facile strategy for preparation of novel and stable Cr-doped $SrTiO_3$/g-C_3N_4 hybrid nano composites with enhanced visible light photocatalytic activity, J. Alloys Compd., 647 (2015) 456–462.
[38] S. Deng, X. Liu, N. Chen, D. Deng, X. Xiao, Y. Wang, A highly sensitive VOC gas sensor using p-type mesoporous Co_3O_4 nanosheets prepared by a facile chemical coprecipitation method, Sens. Actuators, B, 233 (2016) 615–623.
[39] L. Wang, J. Deng, Z. Lou, T. Zhang, Nanoparticles-assembled Co_3O_4 nanorods p-type nanomaterials: one-pot synthesis and toluene-sensing properties, Sens. Actuators, B, 201 (2014) 1–6.
[40] G. Dai, S. Liu, Y. Liang, T. Luo, Synthesis and enhanced photoelectrocatalytic activity of p–n junction Co_3O_4/TiO_2 nanotube arrays, Appl. Surf. Sci., 264 (2013) 157–161.
[41] X. Xu, X. Sun, H. Han, H. Peng, W. Liu, X. Peng, X. Wang, X. Yang, Improving water tolerance of Co_3O_4 by SnO_2 addition for CO oxidation, Appl. Surf. Sci., 355 (2015) 1254–1260.
[42] J. Mei, S. Zhao, W. Huang, Z. Qu, N. Yan, Mn-promoted Co_3O_4/TiO_2 as an efficient catalyst for catalytic oxidation of dibromomethane (CH_2Br_2), J. Hazard. Mater., 318 (2016) 1–8.
[43] J. González-Prior, R. López-Fonseca, J.I. Gutiérrez-Ortiz, B. de Rivas, Oxidation of 1,2-dichloroethane over nanocube-shaped Co_3O_4 catalysts, Appl. Catal., B, 199(2016) 384–393.
[44] W. Li, H. Jung, N.D. Hoa, D. Kim, S.K. Hong, H. Kim, Nanocomposite of cobalt oxide nanocrystals and single-walled carbon nanotubes for a gas sensor application, Sens. Actuators, B, 150 (2010) 160–166.
[45] Y. Guo, B. Xu, F. Qi, A novel ceramic membrane coated with MnO_2–Co_3O_4 nanoparticles catalytic ozonation for benzophenone-3 degradation in aqueous solution: fabrication, characterization and performance, Chem. Eng. J., 287 (2016) 381–389.
[46] T. Hong, Z. Liu, X. Zheng, J. Zhang, L. Yan, Efficient photoelectrochemical water splitting over Co_3O_4 and Co_3O_4/Ag composite structure, Appl. Catal., B, 202 (2017) 454–459.
[47] Z. Fan, Z. Zhang, W. Fang, X. Yao, G. Zou, W. Shangguan, Low-temperature catalytic oxidation of formaldehyde over Co_3O_4 catalysts prepared using various precipitants, Chin. J. Catal., 37 (2016) 947–954.
[48] G. Chen, X. Si, J. Yu, H. Bai, X. Zhang, Doping nano-Co_3O_4 surface with bigger nanosized Ag and its photocatalytic properties for visible light photodegradation of organic dyes, Appl. Surf. Sci., 330 (2015) 191–199.
[49] X.P. Qiu, J.S. Yu, H.M. Xu, W.X. Chen, W. Hu, G.L. Chen, Interfacial effects of the Cu_2O nano-dots decorated Co_3O_4 nanorods array and its photocatalytic activity for cleaving organic molecules, Appl. Surf. Sci., 382 (2016) 249–259.
[50] C. Dong, X. Xiao, G. Chen, H. Guan, Y. Wang, Synthesis and photocatalytic degradation of methylene blue over p-n junction Co_3O_4/ZnO core/shell nanorods, Mater. Chem. Phys., 155 (2015) 1–8.
[51] M.K. Sahu, R.K. Patel, Novel visible-light-driven cobalt loaded neutralized red mud (Co/NRM) composite with photocatalytic activity toward methylene blue dye degradation, J. Ind. Eng. Chem., 40 (2016) 72–82.
[52] Y. Wang, L. Zhou, X. Duan, H. Sun, E.L. Tin, W. Jin, S. Wang, Photochemical degradation of phenol solutions on Co_3O_4 nanorods with sulfate radicals, Catal. Today, 258 (2015) 576–584.
[53] S. Fan, X. Liu, Y. Li, E. Yan, C. Wang, J. Liu, Y. Zhang, Non-aqueous synthesis of crystalline Co_3O_4 nanoparticles for lithium-ion batteries, Mater. Lett., 91 (2013) 291–293.
[54] R.K. Sharma, R. Ghose, Synthesis of Co_3O_4–ZnO mixed metal oxide nanoparticles by homogeneous precipitation method, J. Alloys Compd., 686 (2016) 64–73.
[55] X. Chi, L. Chang, D. Xie, J. Zhang, G. Du, Hydrothermal preparation of Co_3O_4/graphene composite as anode material for lithium-ion batteries, Mater. Lett., 106 (2013) 178–181.
[56] M. Mansournia, N. Rakhshan, Amine ligand-based hydrothermal synthesis of Co_3O_4 nanoparticles, characterization and magnetic study, J. Mol. Struct., 1125 (2016) 714–720.
[57] S. Farhadi, Z. Heydari-Chegeni, M. Mousavi, Facile template-free hydrothermal synthesis of Co_3O_4 hollow microspheres constructed by nanoparticles using $[Co(NH_3)_4CO_3]NO_3$ and their photocatalytic activity, J. Alloys Compd., 692 (2017) 923–933.